Mode-Matched Ion-Exchanged Glass-Waveguide Bridge for High-Performance Dense Wavelength Division Multiplexer

Jizuo Zou, Feng Zhao, *Member, IEEE*, and Ray T. Chen, *Fellow, IEEE, Fellow, OSA*

***Abstract*—Data bit rate, 1-dB passband, and device dimensions are the key properties of dense wavelength division multiplexing (WDM) devices. For blazed-grating-based dense WDM devices, analysis shows that all these three properties can be enhanced by reducing the output fiber-array channel spacing. In this paper, we propose an ion-exchanged glass waveguide to reduce the output channel spacing. To fabricate the low-loss fiber-compatible waveguide, a field-assisted ion-exchange process is developed. The waveguides fabricated by this process have a propagation loss of 0.16 dB/cm and a coupling loss to single-mode fiber (SMF) of 0.1 dB. A 47-channel 100-GHz-spacing dense WDM integrated with the glass waveguide is then packaged and demonstrated. The device performance has verified the effectiveness of the proposed solution and the successfulness of the ion-exchanged glass-waveguide technique in this application.**

***Index Terms*—Glass waveguide, ion exchange, pulse broadening, wavelength division multiplexing (WDM).**

I. Introduction

VARIOUS technologies have been applied to carry out wavelength division multiplexing/demultiplexing (WDM/WDDM). These include thin film filters (TFFs) [1], arrayed waveguide gratings (AWGs) [2], [3], fiber Bragg gratings (FBGs) [4], [5], and free-space diffraction-grating-based WDM [6]. These technologies find their applications in different scenarios based on their performance features. Due to the cascade nature, TFF and FBG WDM devices are mainly attractive to the WDM systems in which the channel counts are not large [7]. For dense WDM in long-haul optical communications with channel counts of 40 and larger, AWG and free-space grating-based WDM are the two promising candidates. The major advantage of the AWG technique is the high integration density. However, manufacturing AWG involves a series of complex production processes and compensation of wavefront distortion out of temperature fluctuation [3]. On the other hand, free-space grating-based WDM devices have such features as low loss, low crosstalk, low polarization-dependent loss (PDL), low temperature sensitivity, multimode operation, and multideck application [6].

In this paper, we first conduct analysis on three major challenges in free-space blazed-grating-based dense WDM devices, i.e., pulse broadening, 1-dB passband, and device dimensions. Based on the analysis, we fabricate an ion-exchanged single-mode fiber (SMF)-compatible glass-waveguide fan-out to enhance the dense WDM performance. To fabricate the waveguide chip, an electric-field-assisted ion-exchange process in conjunction with a post-thermal annealing is developed to ensure the best waveguide-to-fiber mode match. Then, a 47-channel 100-GHz-spacing dense WDM device integrated with such a glass-waveguide fan-out is demonstrated with the projected performance features. Finally, a summary concludes this paper.

Manuscript received November 30, 2004; revised April 28, 2005.

The authors are with the Microelectronics Research Center, J. J. Pickle Research Campus, The University of Texas at Austin, Austin, TX 78758 USA.

Digital Object Identifier 10.1109/JLT.2005.856283

II. Challenges and Solution of Blazed-Grating-Based Dense WDMs

A. Pulse Broadening

Blazed-grating-based WDM/WDDM usually has a Littrow structure [8], as shown in Fig. 1, where G is the blazed grating with a blazing angle of θ, and L is the collimating and focusing lens. The endface of the fiber array that consists of both input and output fibers is placed on the focal plane of lens L. Here, we assume the upper channel of the fiber array is the input, and the rest are the outputs. The whole system works as a WDDM unit. The wavelength-multiplexed light from the input fiber is collimated by lens L. When the collimated light hits on the grating and is diffracted, the diffracted light beam of each wavelength will propagate in a specific direction. Each of these beams is then focused onto a specific fiber of the fiber array by the same lens L. As a result, all the wavelengths are separated into different output channels. If we invert the input and the outputs, the device functions as a WDM unit that combines various input wavelengths into one output channel. For different output channels that have a frequency on the International Telecommunication Union (ITU) grid, the separations between adjacent channels are not equal because of the nonlinear dispersion of the grating [9]. In such a case, the fiber array should be custom designed to have nonuniform channel spacing to ensure best coupling efficiency.

In optical communication systems, the signal carriers are light pulses. These pulses will be broadened when they go through a WDM/WDDM device and therefore, the data-transmission bit rate will be limited. As shown in Fig. 1, the wavefront of the collimated input light pulse is perpendicular to the optical axis. However, after diffraction by the grating, the wavefront is tilted and the lower part of the light beam is delayed compared to the upper part. Once the optical pulse

0733-8724/$20.00 © 2005 IEEE

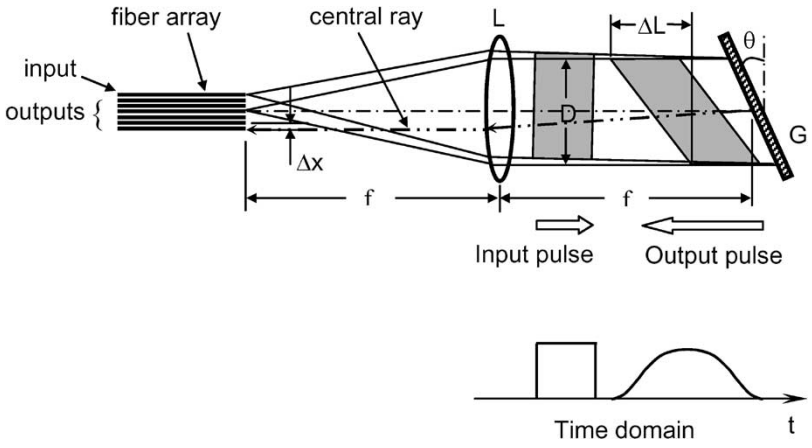

Fig. 1. Schematic of blazed grating-based WDM/WDDM with Littrow structure.

is coupled into the output fiber and eventually converted into an electronic signal, the electronic pulse is broadened in the time domain.

The pulse broadening can be calculated using the diffraction equations of the blazed grating. For the Littrow structure, the incident angle θ_1 and the diffraction angle θ_2 of the grating are equal. In our WDM device, these two angles are different because the input and the output light beams are angularly separated. However, the difference is small. For convenience, we set $\theta_1 = \theta_2 = \theta$ in our analysis. With this assumption, the maximum optical path delay is

$$\Delta L = 2D \tan\theta \approx 4(\mathrm{NA}) f \tan\theta \tag{1}$$

where D is the diameter of the collimated light beam, NA is the numerical aperture of the input fiber, and f is the focal length of lens L. The grating diffraction equation is

$$d(\sin\theta_1 + \sin\theta_2) = 2d\sin\theta = m\lambda \tag{2}$$

where d is the grating period, m is the diffraction order, and λ is the wavelength. Then, we can obtain the angular dispersion

$$\frac{d\theta_2}{d\lambda} = \frac{m}{d\cos\theta_2} = \frac{2d\sin\theta}{d\lambda\cos\theta} = \frac{2\sin\theta}{\lambda\cos\theta} = \frac{2}{\lambda}\tan\theta. \tag{3}$$

The channel-to-channel spacing of the output fiber array on the focal plane of lens L is given by

$$\Delta x \approx f\frac{d\theta_2}{d\lambda}\Delta\lambda = \Delta\lambda\frac{2}{\lambda} f\tan\theta \tag{4}$$

where $\Delta\lambda$ is the channel spacing in wavelength domain. Therefore

$$f\tan\theta \approx \frac{\lambda\Delta x}{2\Delta\lambda}. \tag{5}$$

Finally

$$\Delta L \approx 4(\mathrm{NA})\frac{\lambda\Delta x}{2\Delta\lambda} = 2(\mathrm{NA})\lambda\frac{\Delta x}{\Delta\lambda}. \tag{6}$$

From (6), we can see that for a Littrow setup, the maximum optical path delay induced by the grating depends on the numerical aperture NA, the wavelength λ and the ratio $\Delta x/\Delta\lambda$.

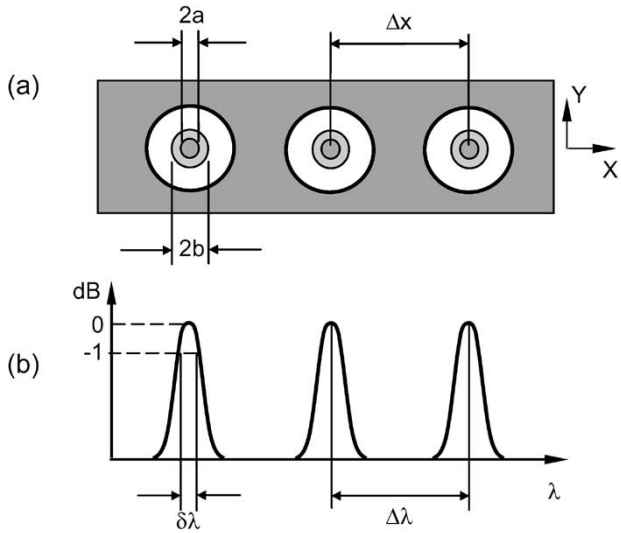

Fig. 2. Definition of 1-dB passband of the WDM device. (a) End face of the fiber array. (b) Output spectrum.

To reduce ΔL, we can decrease the numerical aperture NA and/or the ratio $\Delta x/\Delta\lambda$. Since dense WDM has much larger $\Delta x/\Delta\lambda$ value than coarse WDM, the pulse broadening is also more serious. For example, if NA $= 0.14$ (Corning SMF-28), $\lambda = 1550$ nm, $\Delta x = 127$ μm (standard fiber-array pitch), and $\Delta\lambda = 0.8$ nm (channel spacing of 100 GHz at 1550 nm), the maximum optical path delay is about 68.9 mm, which is equivalent to a broadening of 0.23 ns in the time domain. This broadening will limit the data bit rate to less than 5 Gbit/s.

B. 1-dB Passband

The 1-dB passband is another key parameter of a WDM device. It is the wavelength span measured on the output spectrum when the power drops 1 dB from the peak for a certain channel. This parameter gives the wavelength tolerance of the light source. Larger 1-dB passband means less demanding on the wavelength stability of WDM lasers. Fig. 2(a) shows the endface of the SMF array on which the output light beams are focused by the lens (refer to Fig. 1). The small circle in the center of each fiber denotes the mode profile of that fiber, while the large circle represents the image spot of the output light

beam. When the wavelength changes, the image spot will move along the lateral direction (X), and the coupling efficiency to the output fiber will change. The coupling efficiency can be evaluated by overlap integration between the fiber mode electric field E_f and the image spot electric field E_i [10]:

$$I = \frac{\left(\iint_{-\infty}^{+\infty} E_f E_i \mathrm{d}x\mathrm{d}y\right)^2}{\left(\iint_{-\infty}^{+\infty} E_f^2 \mathrm{d}x\mathrm{d}y\right)\left(\iint_{-\infty}^{+\infty} E_i^2 \mathrm{d}x\mathrm{d}y\right)}. \tag{7}$$

Assume both E_f and E_i have a Gaussian shape with full width at 1/e of the peak of $2a$ and $2b$, respectively, and their lateral center separation is X. Then, the normalized coupling efficiency as a function of X is

$$\overline{I} = \mathrm{e}^{-\frac{X^2}{(a^2+b^2)}} \tag{8}$$

which is also Gaussian.

Since each X value corresponds to a specific wavelength, (8) represents the output spectrum, which is illustrated in Fig. 2(b).

If we use a diffraction-limited lens in the WDM device as shown in Fig. 1, the geometrical aberration can be neglected. Then, the output image profile can be calculated by convoluting the fiber mode profile with the diffraction pattern of the lens aperture [11]. The diffraction pattern of the lens aperture has a full width of $0.84\lambda/\mathrm{NA}$ with a Gaussian approximation [12]. Therefore, the output image spot has a full width of

$$2b = \sqrt{(2a)^2 + \left(\frac{0.84\lambda}{\mathrm{NA}}\right)^2}. \tag{9}$$

The 1-dB passband can be calculated from (8)

$$\delta\lambda = 0.68\sqrt{2a^2 + \left(\frac{0.42\lambda}{\mathrm{NA}}\right)^2}\left(\frac{\Delta\lambda}{\Delta x}\right). \tag{10}$$

Sometimes a 3-dB passband is also used as a WDM specification. The calculated 3-dB passband equals 1.73 times of the 1-dB passband.

From (10), we can find that the 1-dB passband is determined by the values of fiber mode field diameter $2a$, NA, and ratio $\Delta\lambda/\Delta x$. To have a larger 1-dB passband, we should use fibers with larger mode field diameter and smaller, and/or increase the $\Delta\lambda/\Delta x$ ratio. If $\mathrm{NA} = 0.14$, $2a = 10$ μm, and $\Delta\lambda/\Delta x = 0.8$ nm/127 μm, the 1-dB and 3-dB passbands will be about 0.04 and 0.07 nm, respectively, for a 0.8-nm (100-GHz)-channel-spacing WDM.

C. Device Dimensions

The device size is always an important issue for integrated optical devices. To achieve high reliability and high integration density, both the design and fabrication should be optimized to reduce the whole device size as much as possible. For blazed-grating-based WDM devices, one design rule is the telecentric arrangement of the optics. As shown in Fig. 1 again, both the endface of the fiber array, and the the center of the grating are on the focal planes of lens L. With this telecentric arrangement, the central rays of the output light cones are always normal to the endface of the fiber array, and the best coupling efficiency to the output fiber can be achieved. That is, the distance from the fiber array to the grating center is twice the focal length of lens L if the lens thickness is neglected. On the other hand, the beam diameter of the collimated light is also proportional to the focal length of lens L. By reducing the focal length of lens L, both the device length and the lens diameter can be reduced, resulting in a three-dimensional shrinkage of the whole device.

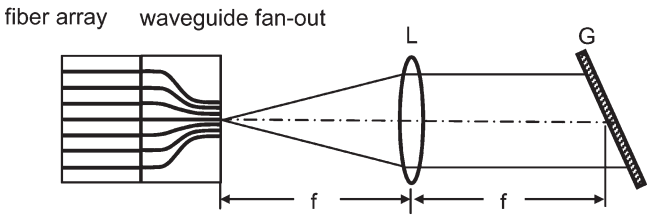

Fig. 3. Blazed-grating dense WDM with ion-exchanged glass-waveguide fan-out.

The required focal length is

$$f = \frac{\left(\frac{\Delta x}{\Delta\lambda}\right)}{\left(\frac{d\theta_2}{d\lambda}\right)}. \tag{11}$$

The lower term on the right-hand side of (11) is the angular dispersion of the grating. Once the grating is selected, this term will be fixed. Therefore, the focal length f is only determined by the ratio $\Delta x/\Delta\lambda$. To reduce the focal length, the output fiber-to-fiber pitch should be decreased.

D. Solution: Ion-Exchanged Glass-Waveguide Fan-Out

From the above analyses, the three challenges in a grating-based dense WDM device all rely on one parameter, the output fiber-to-fiber spacing. By reducing this spacing, the pulse broadening and the device dimensions can be reduced proportionally, and the 1-dB passband can be increased proportionally. Standard SMF array has a pitch size of 250 or 127 μm. To effectively reduce the pitch size, we propose to insert a piece of ion-exchanged glass-waveguide fan-out chip in front of the standard fiber array. The waveguide fan-out consists of curved channel waveguides to shrink the channel spacing. This concept has been introduced to couple light from fiber arrays to detector arrays [13]. In our waveguide fan-out, the waveguide channel spacing has a value of about 19 μm at the end that collects the diffracted output light and 127 μm at the other end that connects to the standard fiber array. The configuration of such a dense WDM is shown in Fig. 3.

Ion-exchanged glass waveguides have a lot of advantages compared with other waveguide technologies. First, the refractive index of glass can be very close to that of fibers, and a perfect match of the waveguide mode with conventional SMF is possible. Second, for most optical glasses, the attenuation due to absorption at telecom wavelength is very low. Third, most glasses have negligible birefringence. Finally and most attractively, the ion-exchange process is simple and reproducible. For the waveguide fan-out in the dense WDM device shown in Fig. 3, the crucial properties include propagation loss, coupling

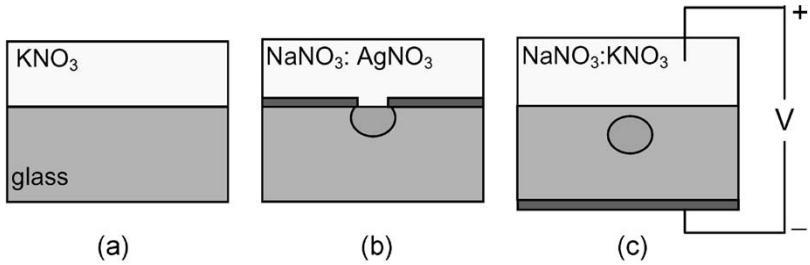

Fig. 4. Ion exchange for SMF-compatible waveguide fabrication. (a) K^+–Na^+ ion exchange. (b) Ag^+–Na^+ ion exchange. (c) Field-assisted waveguide burial.

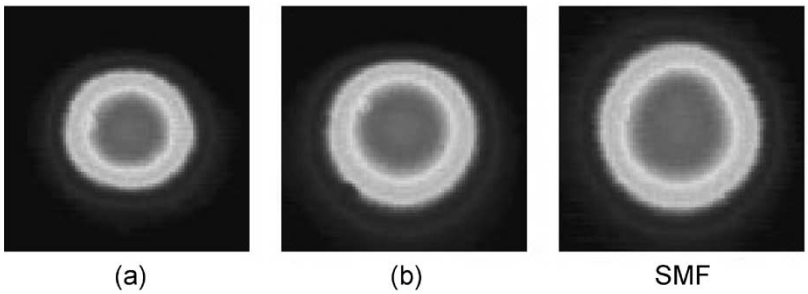

Fig. 5. Mode profiles of buried waveguide (a) before annealing and (b) after 24 h of annealing at 320 °C.

loss to SMF, PDL, bending loss, and crosstalk between adjacent channels. In the following session, a field-assisted ion-exchange process will be introduced to fabricate the waveguide chip.

III. Electric-Field-Assisted Ion Exchange for SMF-Compatible Waveguide Fabrication

Mechanisms, process details, and applications of ion-exchanged glass waveguides can be found in many publications [14], [15]. At elevated temperature (usually 300–500 °C), the sodium ions Na^+ inside glass materials can be interchanged by other ions such as K^+ or Ag^+ through thermal diffusion if the glass is in contact with sources that contain these ions. The K^+ or Ag^+ ions cause a higher refractive index of glass than Na^+ ions. If a masking layer is constructed on the glass surface to define channel regions that will allow the ion exchange to occur, then channel waveguides can be formed. In our case, we use BK7 as the glass material, which has desired optical properties at a 1550-nm wavelength window and low sodium concentrations, which is necessary for single-mode waveguide fabrication.

The whole ion-exchange process consists of three consecutive steps, as shown in Fig. 4. The combination of the first two steps is a two-step thermal K^+–Na^+ and Ag^+–Na^+ ion exchange, which has been investigated in detail in our earlier report [16]. During the first K^+–Na^+ ion exchange, bare glass wafers were dipped into pure molten KNO_3 at 400 °C for 80 min. After that, the glass wafers were cleaned and a 200-nm-thick Al mask layer was deposited and microlithographically patterned on the top surface. During the second Ag^+–Na^+ ion exchange, the masked wafers were dipped into a mixture of $AgNO_3$: $NaNO_3$ (mole ratio 0.02:1) at 320 °C for 5 h. The channel mask width is 3 μm. The major advantages of this two-step method, when compared with conventional one-step Ag^+–Na^+ ion exchange, are the small side diffusion and partial burial of the waveguides.

Since the waveguides are shallow from the glass surface, the mode field profiles are not circular and thus, the coupling loss to SMF is high. To solve this problem, a third-step electric-field-assisted ion exchange was conducted, as in Fig. 4(c). Prior to this step, the Al masking layer was etched away and another 400-nm-thick Al film was deposited on the backside of the glass to form the cathode. On the top surface of the waveguides, a mixture of $NaNO_3$: KNO_3(mole ratio of 60:40) was used as the anode. The temperature of this field-assisted process was 260 °C. During the ion-exchange process, the Na^+ ions in the melt were driven into the glass by the electric field and at the same time, the Na^+ and Ag^+ ions inside the glass migrated toward the cathode. As a result, buried waveguides were obtained. In our experiment, after 45 min of burial with a current density of 0.3 mA/cm^2, the depth of the waveguide mode was obtained to be about 4.2 μm from the glass surface. Fig. 5(a) shows the mode field image, which has a circular profile shape. Since the mode field diameter of this buried waveguides is smaller than that of SMF, we annealed the waveguides for 24 h at 320 °C. The mode field image after this annealing is shown in Fig. 5(b). Calculation has shown that the mismatch between this waveguide mode and the standard SMF mode is about 0.1 dB. Based on this mode profile and the Gaussian model presented in [17], we calculated that the peak refractive index contrast is about 0.006. Fig. 6 presents the measured waveguide propagation loss and coupling loss for four single-mode channel waveguides, with average values of 0.16 dB/cm and 0.3 dB, respectively. The difference between the measured coupling loss and the calculated result is caused by nonperfect alignment during the measurement and nonperfect polishing of the waveguide endfaces. For 5-cm-long waveguides, the PDL is lower than 0.1 dB.

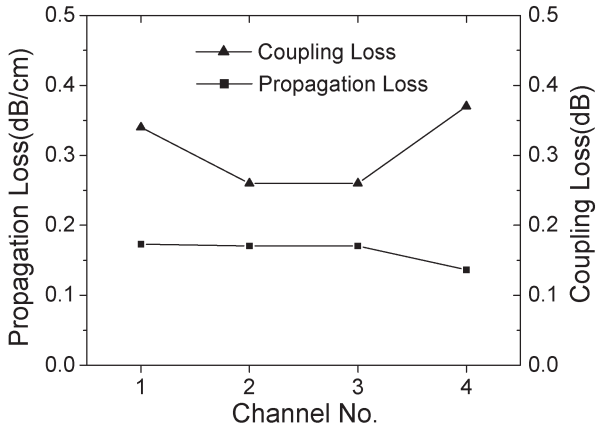

Fig. 6. Propagation loss and coupling loss to SMF of buried waveguides after 24 h of annealing at 320 °C.

IV. Dense WDM Design and Packaging

A 48-channel SMF array with pitch size of 127 μm was used in the dense WDM device. With one channel as the multiplexed channel, 47 channels are available for the demultiplexed channels. The device can cover most of the C-band wavelength window with a channel spacing of 100 GHz. For convenience, we design our dense WDM to cover the frequency from 191.1 to 195.7 THz on the ITU grid, which corresponds to the wavelength range from 1568.77 to 1531.90 nm.

The blazed grating that we used for the dense WDM device has a groove density of 600 l/mm and the blazing occurs at the first diffraction order. Optimized for telecom applications, the diffraction efficiency curves of s- and p-waves intercept at the wavelength of 1550 nm, with an efficiency value of 78%. Within the wavelength range that our WDM device covers, the maximal PDL introduced by the grating is less than 0.1 dB. A doublet lens with broadband near-infrared antireflection coatings was used to collimate and focus the laser beams. The effective focal length and the clear aperture of the lens are 35 and 12 mm, respectively. Optical modeling found that the aberration-induced image size is about 1/3 of the diffraction limit. The coupling efficiency of the focused image to a standard SMF is 83%–88% for different channels.

The channel waveguides on the waveguide fan-out have a cosine-defined S-bend structure, which has the lowest bending loss according to theoretical calculations [17] and our experimental results. The channel spacings at the small end of the waveguide are not equal due to the nonlinear grating dispersion and the values are listed in Table I. The channel spacing at the other end interfacing with a fiber array is 127 μm. The length of the whole chip is 12 mm. The minimum radius of curvature of the S-bend waveguides is 14 mm, which causes negligible bending losses. The waveguide was fabricated using the process described in the previous section. The measured insertion losses of the 48 channels with both the input and output coupled with SMF are from 0.7–1.0 dB, with an average of 0.8 dB. The crosstalk between adjacent channels is lower than -26 dB.

The WDM was aligned and packaged on a Newport AutoAlign Packaging system with a linear positioning accuracy of 0.05 μm. The alignment of the waveguide chip with the fiber array was accomplished by aligning only the first and the forty-eighth channels. Then, the waveguide was moved away from the fiber array and a thin layer of UV-cured epoxy was applied on the endfaces of the waveguide chip and the fiber array. After that, the waveguide chip was moved back to the aligned position and the epoxy was cured by UV light. To obtain a strong and robust bonding, another piece of BK7 substrate was attached to the backside of the whole piece using UV-cured epoxy. The grating was mounted on a mini-mirror mount, and the bonded waveguide assembly was easily aligned to the grating by angular adjustments. All the mechanical mounting parts were designed with a hard contact configuration to ensure mechanical stability. The packaged 47-channel 100-GHz-spacing dense WDM is shown in Fig. 7. The overall device dimensions are $5.3'' \times 1.6'' \times 1.2''$.

TABLE I
Channel Spacings of the Waveguide at the End Facing the Collimating Lens

Channel	Spacing (μm)	Channel	Spacing (μm)	Channel	Spacing (μm)	Channel	Spacing (μm)
1	19.57	13	19.27	25	18.96	37	18.65
2	19.54	14	19.24	26	18.94	38	18.63
3	19.52	15	19.21	27	18.91	39	18.60
4	19.49	16	19.19	28	18.88	40	18.58
5	19.47	17	19.16	29	18.86	41	18.55
6	19.44	18	19.14	30	18.83	42	18.52
7	19.42	19	19.11	31	18.80	43	18.50
8	19.39	20	19.09	32	18.78	44	18.47
9	19.37	21	19.06	33	18.76	45	18.45
10	19.34	22	19.04	34	18.73	46	18.42
11	19.31	23	19.01	35	18.70	47	
12	19.29	24	18.98	36	18.68		

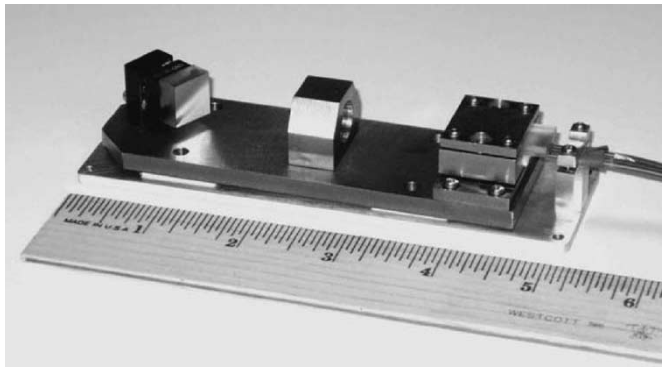

Fig. 7. Forty-seven-channel dense WDM integrated with ion-exchanged glass waveguide.

V. Dense WDM Performance

The 47-channel dense WDM was characterized as a demultiplexer, in which input light was coupled into the multiplexed channel, and outputs from demultiplexed channels were coupled into a digital power meter or an optical spectrum analyzer (OSA). A tunable laser was used as the light source for the measurement of the insertion loss and crosstalk, while a broadband amplified spontaneous emission (ASE) light source was used to get the output spectra for the 1-dB and 3-dB passband measurements. The pulse-broadening effect of the dense WDM device was investigated using a modulated laser signal as the

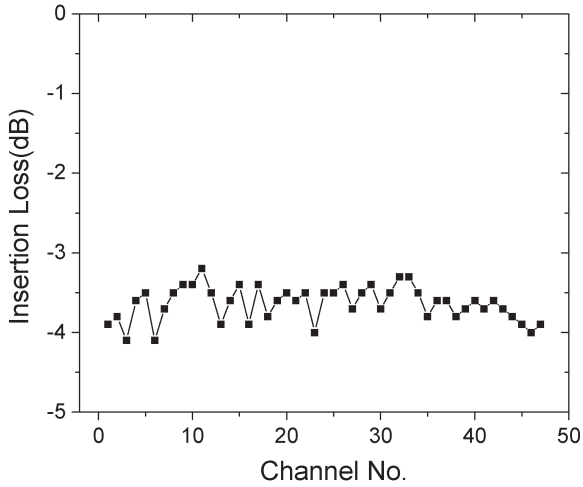

Fig. 8. Insertion loss of the 47-channel dense WDM.

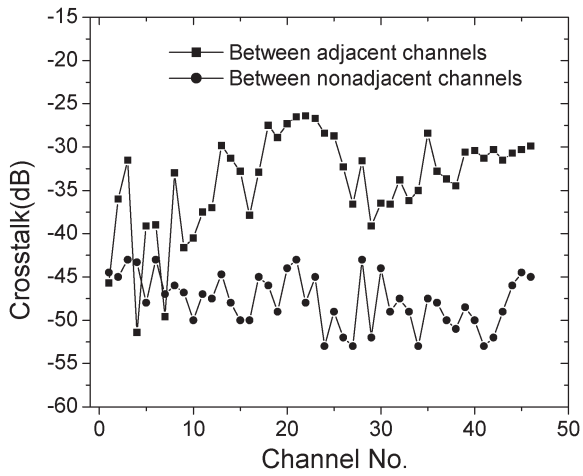

Fig. 9. Crosstalk between adjacent channels and nonadjacent channels.

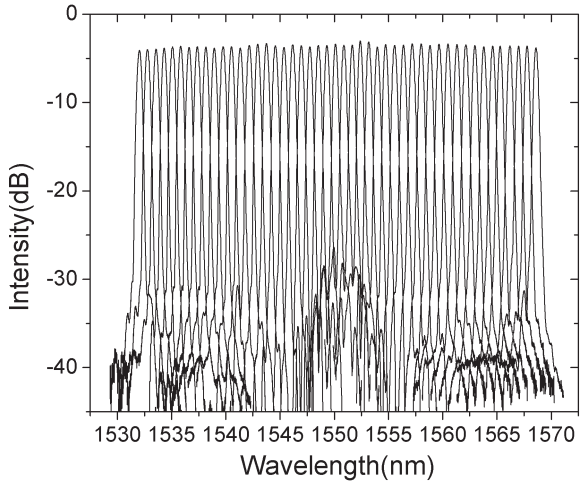

Fig. 10. Output spectra of the 47-channel dense WDM.

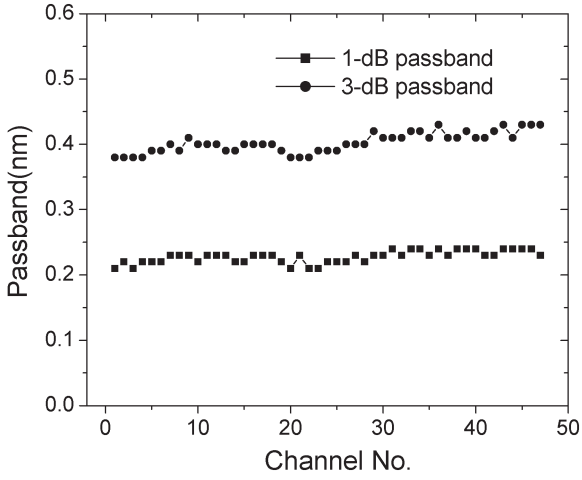

Fig. 11. 1-dB and 3-dB passbands of the 47-channel dense WDM.

input. Both the input and the output pulse profiles were captured using a digital oscilloscope.

The insertion losses of the dense WDM device are shown in Fig. 8. For the 47 channels, the insertion loss varies from -3.2 to -4.1 dB with an average of -3.6 dB. The insertion loss can be reduced to less than -3 dB if gold is used as the reflection coating of the grating instead of aluminum and antireflection coatings are deposited at the glass–air interface of the waveguides.

The measured crosstalks between adjacent and nonadjacent channels are presented in Fig. 9. The largest crosstalk between adjacent channels is -26.5 dB, which occurs between the central channels of 23 and 24. The nonadjacent channel crosstalks are lower than -42 dB for all of the 47 channels.

1-dB and 3-dB passbands were measured from the spectrum of each channel, with the ASE light source as the input. Fig. 10 shows the dense WDM spectra and Fig. 11 presents the quantitative results of the 1-dB and 3-dB passbands. The 1-dB passband varies from 0.21 to 0.24 nm for different channels, with an average of 0.23 nm. In the frequency domain, this average 1-dB passband corresponds to 28.5 GHz. The 3-dB passband is between 0.38 and 0.43 nm, with an average of 0.40 nm or 50 GHz in the frequency domain. Both 1-dB and 3-dB passbands are a little bit larger for the higher number channels than the lower number channels. This is caused by the unequal waveguide spacing at the small end of the waveguide fan-out. The calculated 1-dB passband using (10) varies from 0.23 to 0.24 nm for the channels from the first to the forty-seventh. We can see that the measured data are very close to the calculated ones.

The pulse-broadening effect was investigated with light pulses coupled into the input channel. The input and the output optical pulse profiles were recorded as in Fig. 12(a) and (b), respectively. The amplitude difference between these two pulses was caused by the insertion loss. Due to the limitation of our signal source, the shortest optical pulse we can obtain has a full-width at half-maximum (FWHM) of 123 ps. With such an input signal, the FWHM of the output pulse is about 130 ps. By deconvoluting the output pulse with respect to the input pulse, the pulse broadening can be calculated to be about 40 ps. Compared to the calculated result of 0.23 ns when a standard 127-μm-spacing fiber array is used to couple the light out, we can find that the pulse broadening has been significantly suppressed by the waveguide fan-out.

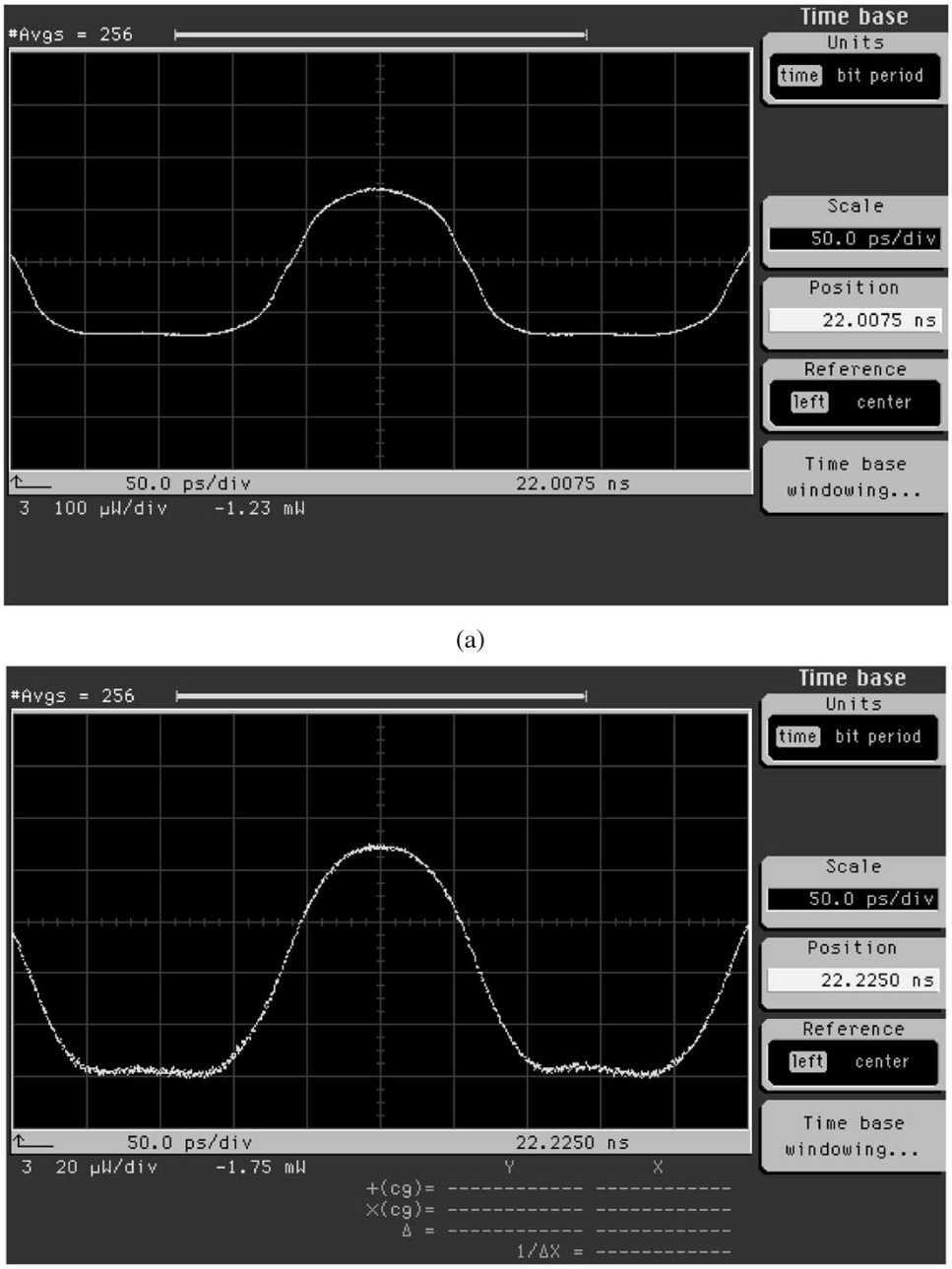

Fig. 12. Pulse-broadening effect of the 47-channel dense WDM: (a) Input optical pulse and (b) output optical pulse.

We did not conduct the measurement of PDL and temperature sensitivity of this device, since these results have been reported in earlier publications from our group [6], [9] for WDM devices using similar blazed grating and similar Littrow structure as the one we reported here.

VI. Summary

In this paper, we first analyzed major challenges of the blazed-grating-based dense WDM devices. These challenges include pulse-broadening effect, 1-dB passband, and device dimensions. To overcome these challenges, we proposed integrating an ion-exchanged glass waveguide into the device. To fabricate this waveguide chip, we successfully developed a field-assisted ion-exchange process. Using this process, single-mode channel waveguides with propagation loss of 0.16 dB/cm and coupling loss to SMF of 0.1 dB have been fabricated. The waveguide was then successfully bonded with a standard 48-channel fiber array and a 47-channel 100-GHz-spacing dense WDM device has been demonstrated. The dense WDM device has an average insertion loss of -3.6 dB, 1-dB passband of 0.23 nm, and pulse broadening of 40 ps. The improvements of the dense WDM performance by the waveguide are consistent with the predictions. In addition, with accurate channel spacings at the end of the waveguide chip that collects the output light beams, the nonlinear problem of the

output-beam positions is solved, and therefore, a custom-designed fiber array is not required. Further improvement of the WDM device is possible with more efforts to reduce the channel spacing at the smaller end of the waveguide fan-out. Our future work will include the tapering of the waveguides by gradually changing annealing temperature along the waveguide to shrink the mode field dimensions and inserting air gap between waveguides. With both approaches, the channel spacing can be reduced significantly without introducing higher crosstalk.

REFERENCES

[1] Y. Hibino, "Passive optical devices for photonic networks," *IEICE Trans. Commun.*, vol. E83-B, no. 10, pp. 2178–2190, Oct. 2000.

[2] H. Takahashi, S. Suzuki, K. Kato, and I. Nishi, "Arrayed waveguide grating for wavelength division multi/demultiplexer with nanometer resolution," *Electron. Lett.*, vol. 26, no. 2, pp. 87–88, Jan. 1990.

[3] K. Okamoto, Y. Inoue, T. Tanaka, and Y. Ohmori, "Silica-based planar lightwave circuits for WDM applications," *IEICE Trans. Electron.*, vol. E81-C, no. 8, pp. 1176–1186, Aug. 1998.

[4] K. O. Hill, B. Maro, F. Bilodeau, D. C. Johnson, and J. Albert, "Bragg gratings fabricated in monomode photosensitive fiber by UV exposure through a phase mask," *Appl. Phys. Lett.*, vol. 62, no. 10, pp. 1035–1037, Mar. 1993.

[5] D. C. Johnson, K. O. Hill, F. Bilodeau, and S. Faucher, "New design concept for a narrowband wavelength-selective optical tap and combiner," *Electron. Lett.*, vol. 23, no. 13, pp. 668–669, Jun. 1987.

[6] F. Zhao, Y. Zhang, J. Zou, Z. Shi, B. Bihari, E. Frietman, X. Deng, J. Qiao, Z. Shi, and R. T. Chen, "Wavelength division multiplexers/demultiplexers for optical interconnects in massively parallel processing," *Opt. Eng.*, vol. 42, no. 1, pp. 273–280, Jan. 2003.

[7] F. Zhao, J. Qiao, X. Deng, J. Zou, B. Guo, R. Collins, V. Villavicencio, K. K. Chang, J. W. Horwitz, B. Morey, and R. T. Chen, "Reliable grating-based wavelength division (de)multiplexers for optical networks," *Opt. Eng.*, vol. 40, no. 7, pp. 1204–1211, Jul. 2001.

[8] J. W. Horwitz *et al.*, "Highly reliable 32-channel wavelength division demultiplexer," in *Proc. SPIE*, San Jose, CA, 2000, vol. 3949, pp. 82–89.

[9] J. Qiao, F. Zhao, R. T. Chen, J. W. Horwitz, and W. W. Morey, "A thermalized low-loss Echelle-grating-based multimode dense wavelength division demultiplexer," *Appl. Opt.*, vol. 41, no. 31, pp. 6567–6575, Nov. 2002.

[10] D. Marcuse, *Light Transmission Optics*. New York: Van Nostrand Reinhold, 1982.

[11] J. W. Goodman, *Introduction to Fourier Optics*. New York: McGraw-Hill, 1996.

[12] M. Born and E. Wolf, *Principles of Optics*. New York: Pergamon, 1993.

[13] P. Kern, J. P. Berger, P. Haguenauer, F. Malbet, and K. Perraut, "Planar integrated optics contribution to instrumentation for interferometry," in *Proc. SPIE*, Munich, Germany, 2000, vol. 4006, pp. 974–985.

[14] R. V. Ramaswamy and R. Srivastava, "Ion-exchanged glass waveguides: A review," *J. Lightw. Technol.*, vol. 6, no. 6, pp. 984–1002, Jun. 1988.

[15] S. I. Najafi, *Introduction to Glass Integrated Optics*. Boston, MA: Artech House, 1992.

[16] J. Zou, F. Zhao, and R. T. Chen, "Two-step K^+–Na^+ and Ag^+–Na^+ ion-exchanged glass waveguides for C-band applications," *Appl. Opt.*, vol. 41, no. 36, pp. 7620–7626, Dec. 2002.

[17] H. F. Schlaak, A. Branderburg, and G. Sulz, "Integrated optical circuits with curved waveguides," in *Integrated Optical Circuit Engineering III*, R. T. Kersten, Ed., Innsbruck, Austria, 1986, vol. 651, pp. 38–45.

Jizuo Zou received the Ph.D. degree in electrical and computer engineering from the University of Texas at Austin in 2004.

His research interest includes wavelength division multiplexers/demultiplexers, optical waveguides, and photonic packaging.

Feng Zhao (S'90–M'92), photograph and biography not available at the time of publication.

Ray T. Chen (M'91–SM'98–F'04) received the B.S. degree in physics from the National Tsing Hua University, Hsinchu, Taiwan, in 1980, and the M.S. degree in physics and the Ph.D. degree in electrical engineering in 1983 and 1988, both from the University of California.

He is the Temple Foundation Endowed Professor at the University of Texas (UT) at Austin. He joined the UT Austin as a Member of the faculty to start optical interconnect research program in the ECE Department in 1992. Prior to his UT's professorship, he worked as a Research Scientist, Manager, and Director of the Department of Electrooptic Engineering in Physical Optics Corporation in Torrance, CA, from 1988 to 1992. He also served as the CTO/Founder and Chairman of the Board of Radiant Research from 2000 to 2001 where he raised $18 million A-Round funding to commercialize polymer-based photonic devices. His research work has been awarded with more than 80 research grants and contracts from sponsors such as DOD, NSF, DOE, NASA, the State of Texas, and the private industry. His research topics are focused on two main subjects: polymer-based guided-wave optical interconnection and packaging and true time delay (TTD) wideband phased array antenna (PAA). Experiences garnered through these programs in polymeric material processing and device integration are pivotal elements for the research work reported herein. His group at UT Austin has reported its research findings in more than 400 published papers including over 55 invited papers. He holds 12 issued patents. There are 23 students who received the EE Ph.D. degree from his research group at UT Austin.

Dr. Chen is a Fellow of Optical Society of America (OSA) and SPIE. He was the recipient of the 1987 UC Regent's dissertation fellowship and the 1999 UT Engineering Foundation Faculty Award for his contributions in research, teaching, and services. Back to his undergraduate years at the National Tsing Hua University, he led a university debate team in 1979, which received the national championship of the national debate contest in Taiwan. He has chaired or been a program committee member for more than 50 domestic and international conferences organized by IEEE, SPIE (The International Society of Optical Engineering), OSA, and PSC. He has served as an Editor or Co-Editor for 18 conference proceedings. He has also served as a Consultant for various federal agencies and private companies and delivered numerous invited talks to professional societies.